Macromolecules

Article

pubs.acs.org/Macromolecules

Cell Dynamics Simulations of Sphere-Forming Diblock Copolymers in Thin Films on Chemically Patterned Substrates

Maria Serral,[†] Marco Pinna,*[,‡] Andrei V. Zvelindovsky,[‡] and Josep Bonet Avalos*[,†]

[†]Department d'Enginyeria Química, Universitat Rovira i Virgili, Tarragona, Av. dels Països Catalans, 26, 43007 Tarragona, Spain

[‡]School of Mathematics and Physics, College of Science, University of Lincoln, Brayford Pool, Lincoln, Lincolnshire LN6 7TS, U.K.

Supporting Information

ABSTRACT: The morphology of sphere-forming block copolymers assembled in thin films on patterned surfaces is theoretically analyzed. The patterns on the lower surface are alternating bands of a given width distinctively attracting or repelling a given block. We find that long-range order can be achieved, and it depends on the commensurability of the characteristic length of the block domains with both band periodicity and slit thickness. The comparison of the simulation results with experimental data shows a very good agreement. Furthermore, we show that the proper selection of the band periodicity and, consequently, of the film thickness permits the system to switch from hexagonal packing to body-centered orthohedra. Therefore, we show that it exists a way to control the formation of long-range ordered structures of different types in this kind of system.

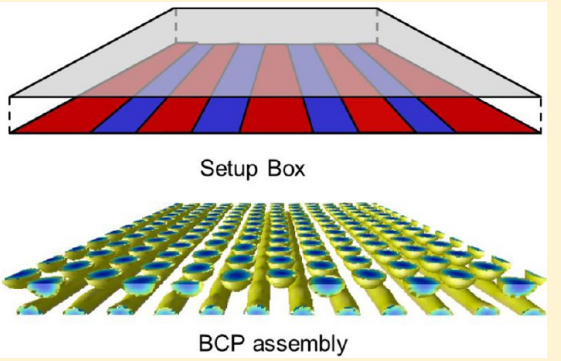

1. INTRODUCTION

Supramolecular structures of nanometric size are of great interest due to potential applications in nanotechnology, which range from nanopatterned surfaces, nanocrystals with exotic optoelectronic properties, to functional foods and pharmacological products.[1−3] The main technological problem is to achieve the control and reliability of the final product when traditional manufacturing processes cannot be downscaled to the nanometric size. Hence, physical systems that spontaneously form supramolecular assemblies under appropriate conditions are so important, as far as they can be externally controlled to produce the desired target structure.[4] Block copolymers (BCP) are one of these valuable materials because of their ability to self-assemble into different nanostructures.[5−9]

In this article we address the problem of how external effects, like the presence of a chemical mask on a surface, affects the two- and three-dimensional structure of thin films of sphere forming BCP. This question was experimentally analyzed by Park et al.,[10] showing some interesting aspects of the self-organization of BCP in the presence of a structured wall. Here we apply cell dynamics simulation (CDS) to widen the range of conditions experimentally analyzed and, more importantly, to infer the relationship between the aforementioned external constraints and the particular features of the structures obtained. We find that the surface pattern allows to selectively produce nonbulk types of structures in BCP films.

BCP consist of blocks of chemically different monomers covalently bond. The simplest systems are (A−B) diblock copolymers. If monomers A and B are highly incompatible, the system can spontaneously segregate into two distinct nanodomains (microphase separation). The size of such nanodomains is on the range between 10 and 100 nm. Depending on the nature of the monomers, such as their degree of polymerization, interaction between the components, and the relative size of each block, these microphases can be either lamellae, cylinders, or spheres, although other more exotic morphologies, like the gyroid phase, can be observed.[11−13]

Morphologies not accessible in the bulk can exist under confinement due to the additional constraints imposed by the surfaces on the system.[14] Constraints can be spatial frustration, preferential attraction of one of the blocks to the walls with respect to the other, and structures at the interfaces, among others. The confinement geometry can hinder the system in one, two, or three dimensions,[15,16] as in confinement in thin films, in cylindrical,[17−20] or spherical pores.[21]

Focusing our attention on thin films, a variety of domain architectures can be obtained influenced by the boundary conditions at both the top and bottom interfaces.[22−25] BCP can serve to pattern large areas of regular arrays of nanostructures for nanolitography, for the synthesis of highly ordered dispersions of inorganic particles. They can be used for semiconductors, magnetic storage media, photonic crystals, and nanostructured membrane applications, among many others.[5−9] Almost invariably, microdomains with a long-range order are required for these applications. However, in real systems long-range order is hindered by a rather degenerate free-energy landscape as well as by the slow diffusion of the polymers in the process of domain reorganization after

Received: October 22, 2015
Revised: January 4, 2016

DOI: 10.1021/acs.macromol.5b02314
Macromolecules XXXX, XXX, XXX−XXX

quench.[26,27] It has been shown that perfectly ordered arrays of domains in thin films of BCP are not expected even at equilibrium, since in a nearly 2-D system the translational order is at best quasi-long-range due to a finite concentration of thermally activated defects.[28,29] Moreover, hexatic phases with no long-range translational order appear at temperatures close to the melting of the structure into a disordered phase of domains.[27] A review on the importance of the spontaneous defects as well as the kinetically arrested imperfections in direct self-assembly of BCP has been recently published by Li and Müller.[30]

Various techniques have been proposed to tailor the arrangements of nanoscale domains, or to accelerate the slow dynamics of the ordering near equilibrium, to produce the aforementioned well-controlled long-range order. One can find the modifications in the supporting substrates, such as topographical or chemical patterning and the application of external fields, like shear or electrical fields.[1,31] For symmetric (lamellae forming) BCP the commensurability between the periodicity of the pattern substrate and the natural length scale of the BCP was found to play an indispensable role to obtain a particular lamellar morphology in thin films.[32] Subsequently, regular almost defect-free linear conformations in the nanoscale could be fabricated.[33−35] As far as the asymmetric block copolymers are concerned, dense arrays of nanocylinders with controlled orientation and enhanced uniformity are obtained using hexagonal arrays of dots chemically patterned on the supporting substrate.[36−39] Square arrays of vertical cylinders, instead of the hexagonal array typically found in bulk, can also be produced using a chemically patterned surface with a square array of spots.[40]

With regards to the sphere-forming BCP in thin films, long-ranged order structures are achieved on topographically modified surfaces forming wells and mesas, which yield crystal-like structures.[41] On the other hand, when assembling spheres in V-shaped grooves, well-ordered domains are obtained with a face-centered cube (FCC) close-packing structure, with the (111) planes of the array parallel to the groove walls.[42] Additionally, hexagonally arranged posts or semidense hole patterns[43,44] can be used to form arrays of spherical domains whose periodicity is larger than the one of the substrate, a phenomenon referred to as *density multiplication*. The orientation and periodicity of the resulting array of spherical microdomains are found to be governed by the commensurability between the BCP microphase characteristic length and the template periodicity. Alternatively, well-aligned spherical domains built using a chemically striped patterned surface, also with a periodicity commensurate with the BCP natural periodicity, were reported.[10] Furthermore, the film thickness is also a key parameter to draw long-range order of spherical BCP domains, as can be inferred from the transitions between the typical 3-D body-centered cube (BCC) arrangement of spheres found in the bulk and the 2-D hexagonal (HEX) arrangement encountered under confinement.[26,45]

Recent efforts have been directed to increase the accuracy of the control over the shapes and dimensions of the equilibrium morphologies.[46,47] The goal is to improve defect-free long-range order arrangements, aiming at obtaining high density multiplication, together with pattern quality rectification and fabrication of new complex structures never found in the bulk.[48−52] Müller et al.[4] recently introduced a new procedure to drive the self-assembly toward desired geometries through a process-directed mechanism in which the kinetics of structure formation is externally led to achieve the sought long-life metastable state.

From the theoretical viewpoint, two main approaches have been widely used to describe the microphase separation of BCP. On the one hand, the self-consistent field theory (SCFT) deals with coarse-grained models of the BCP in which bonded interactions are described as flexible Gaussian chains, while nonbonded interactions are introduced through the mean local densities. Many calculations in 2 and 3 dimensions for relatively small systems have been carried out aiming at understanding the formation of BCP structures.[53−57] In this line, simulations of confined systems, with chemically activated or topographically modified substrates, were performed by several authors.[36,58−61] Although the method permits to keep some molecular details of the chain, SCFT is still a computationally expensive method when large systems are to be studied. Particularly, the dynamic processes involving domain restructuration are very long as compared with the molecular scales of chain reorganization, whose specific consideration is required in a dynamic implementation of the SCFT. Other particulate models, also based on coarse-grained descriptions of the BCP molecules, have also been constructed and used in several studies. Early lattice Monte Carlo simulations of simple models were used to analyze BCP in confined geometries, including also patterned surfaces.[62,63] More recently, it was introduced the so-called *theoretically informed* coarse-grained simulations (TICG),[64,65] which permit the study of the BCP dynamics through dynamic Monte Carlo methods, for instance. Although coarse-grained, this method allows for the study of multicomponent systems, suspended particles, can reproduce thermal fluctuations (i.e., spontaneously generate thermal defects), etc., and still be computationally efficient. Together with the SCFT, TICG approximately described the conformational changes of the BCP chains in the vicinity of a interface. However, the explicit considerations of coarse-grained chain conformations limits the affordability of simulations of large systems or long-time ranges.

On the other hand, Ohta and Kawasaki[66] developed a free-energy functional corresponding directly to the monomer concentration fields, with no explicit reference to microscopic details, except in the definition of the coefficients. Its final form resembles a Ginzburg−Landau functional supplemented with a long-range contribution that accounts for the chain connectivity. From the free-energy functional a diffusive dynamics can be constructed in the spirit of the Cahn−Hilliard−Cook (CHC) equation[67] for systems with a conserved order parameter. This coarse-grained level of description allows to observe the microphase separation phenomena in systems whose dimensions are comparable with the ones experimentally addressed. This method is customarily referred to as cell dynamics simulation.[68,69] In the framework of this method the dynamics and structure of BCP on chemically patterned surfaces have also been studied for cylinder and lamellae forming BCP.[70−75]

However, the theoretical analysis of the self-assembly of spheres on a chemically patterned surface has not been addressed yet. In this article we explore the usefulness of a very simple stripped pattern in guiding the final structure of asymmetric sphere forming BCP in contrast to more sophisticated designs like arrays of spots or other graphoepitaxial techniques. The numerical approach allows us to infer the effect of the commensurability between the pattern periodicity, as well as the slit thickness, and the natural spacing

DOI: 10.1021/acs.macromol.5b02314
Macromolecules XXXX, XXX, XXX−XXX

of the formed structures. The analysis permits us to identify the optimal conditions for defect-free assemblies of several layers of spheres, with different unit cell. The study reveals some keys for a better structure control in the manufacturing at the nanoscale.

The paper is organized as follows. In section 2, we introduce the theoretical background of the CDS and its application to a system implemented on a lattice. Special emphasis is made in deriving the appropriate free-energy functional for the lattice. In section 3, we analyze the theoretical results and compare them with the available experimental data. Predictions for a wider range of conditions are also discussed. Finally, section 4 is devoted to review the main conclusions that can be drawn from our work.

2. MODEL

Cell Dynamics Simulation. The cell dynamics simulation method was introduced to model interface dynamics in phase-separating systems. Theoretically, CDS is based on the Cahn−Hilliard−Cook equation, which is used as the governing differential equation for the time evolution of a conserved order parameter $\Psi(\mathbf{r},t)$.[68,76] The CHC equation can be derived from the balance equation for the order parameter together with the linear relationship between the order parameter flux $\mathbf{J}(\mathbf{r},t)$ and the local chemical potential,[77] eqs 1 and 2, respectively. That is

$$\frac{\partial \Psi(\mathbf{r}, t)}{\partial t} = -\nabla \cdot \mathbf{J}(\mathbf{r}, t) \tag{1}$$

$$\mathbf{J}(\mathbf{r}, t) = -M \nabla \mu(\mathbf{r}, t) \tag{2}$$

The chemical potential can be expressed as a functional derivative of the free energy functional

$$\mu(\mathbf{r}, t) = \frac{\delta F[\Psi]}{\delta \Psi(\mathbf{r}, t)} \tag{3}$$

Hence, the CHC equation is obtained as

$$\frac{\partial \Psi}{\partial t} = M \nabla^2 \left(\frac{\delta F[\Psi]}{\delta \Psi} \right) \tag{4}$$

where M is a phenomenological mobility constant taken as $M = 1$. This choice sets the time scale for the diffusive processes (the dimensionless time is tM/a_0^2, where the lattice cell spacing a_0 is taken as the unit of length). The dynamics of eq 4 is consistent with the mean-field theory and would correspond to a situation with negligible thermal fluctuations, namely, BCP of large molecular weight[78,79] (see the Supporting Information for a discussion on the description of thermal noise in CDS; also see Zvelindovsky and Zatovsky,[80] van Vlimmeren et al.,[81] Knoll et al.,[82] and Horvat et al.[83]).

In CDS, the commonly used expression for the order parameter $\Psi(\mathbf{r},t)$ in terms of the A and B comonomer volume fractions, ϕ_A and ϕ_B, respectively, is[68,69]

$$\Psi(\mathbf{r}, t) = \phi_A(\mathbf{r}, t) - \phi_B(\mathbf{r}, t) + (1 - 2f) \tag{5}$$

where $f = N_A/(N_A + N_B)$ stands for the number fraction of A monomers per chain. The order parameter is then the difference between the local volume fraction of both monomers, plus a constant such that the integral of $\Psi(\mathbf{r},t)$ over the entire volume of the system is 0 by construction. For symmetric copolymers, $f = 1/2$, the constant vanishes.

The necessary condition of equilibrium is given by

$$\left. \frac{\delta F[\Psi]}{\delta \Psi} \right|_{\text{eq}} = 0 \tag{6}$$

with a positive second functional derivative. Equation 6 is not a sufficient condition because the system can be trapped into local metastable minima during its time evolution according to eq 4.

The free energy $F[\Psi]$ (in reduced units such that $kT = 1$) is given by[66,84]

$$F[\Psi(\mathbf{r})] = \int d\mathbf{r} \left\{ \left[H(\Psi) + \frac{D}{2} |\nabla \Psi|^2 \right] + \frac{B}{2} \int d\mathbf{r}' \times G(\mathbf{r} - \mathbf{r}') \Psi(\mathbf{r}) \Psi(\mathbf{r}') - \sum_i s_i(\mathbf{r}) \Psi(\mathbf{r}) \right\} \tag{7}$$

The first term, $H(\Psi)$, contains the local contributions to the free energy, expressed as an expansion in terms of the order parameter, in the spirit of the Ginzburg−Landau theory.[66,85] The expression used in the current analysis is given by[68,86]

$$H(\Psi) = \left[-\frac{\tau}{2} + \frac{A}{2}(1 - 2f)^2 \right] \Psi^2 + \frac{\nu}{3}(1 - 2f) \Psi^3 + \frac{u}{4} \Psi^4 \tag{8}$$

Here, A, ν, and u are phenomenological constants derived by Leibler[85] using the random phase approximation, and τ is proportional to the Flory−Huggins parameter χ, which inversely depends on the temperature T. According to Ohta and Kawasaki,[66,85] the parameter

$$\tau' \equiv -\tau + A(1 - 2f)^2 \tag{9}$$

can be expressed in terms of physical parameters as

$$\tau' = -\frac{1}{2N} \left(N\chi - \frac{\tilde{s}(f)}{4f^2(1 - f)^2} \right) \tag{10}$$

where $\tilde{s}(f)$ is an empirical fitting function whose value is of order of 1.[66]

The surface term, $D|\nabla \Psi|^2/2$, accounts for the free energy necessary to create an interface between A and B. The coefficient D is a positive constant that scales as $D \sim b^2$, where b is the Kuhn segment length of the polymer. The expression for D reads[85]

$$D = \frac{b^2}{48 f(1 - f)} \tag{11}$$

Additionally, chain connectivity introduces a long-range term in eq 7, with the coefficient B that scales as N^{-2}, and reads[66,68,85]

$$B = \frac{9}{(2Nbf(1 - f))^2} \tag{12}$$

where $N = N_A + N_B$ is the total degree of polymerization. This term carries a chain-length dependence. Notice that the Green function $G(\mathbf{r} - \mathbf{r}')$ satisfies $\nabla^2 G(\mathbf{r} - \mathbf{r}') = -\delta(\mathbf{r} - \mathbf{r}')$.[66,68,85,86] It should be mentioned here that this particular form of the Green function was derived for bulk systems. The presence of hard walls is expected to influence the functional form of the Green function due to the reduction of the number of chain conformations when polymers are near an impenetrable surface, as follows from its derivation.[66,85] However, this effect qualitatively does not introduce significant deviations in the predictions, as can be seen from the

DOI: 10.1021/acs.macromol.5b02314
Macromolecules XXXX, XXX, XXX−XXX

comparison with experimental data of related systems later on. For convenience, we define the dimensionless parameters $\tilde{D} = D/a_0^2$ and $\tilde{B} = Ba_0^2$ to be used in the simulations. For simplicity, we write D and B instead of $\tilde{D}$ and $\tilde{B}$ from now on. The parameters in eqs 7−9 are considered as phenomenological constants.

The last term in eq 7, where i denotes either A or B component, takes into account the interaction of the block copolymer with the confining hard walls. In the present case, the walls model surfaces presenting a chemically activated mask. Hence, $s_i(x,y,z)$ is defined as[87,88]

$$s_i(x, y, z) = h_i \phi_i \tilde{\delta}_x \delta_{z,1} \tag{13}$$

$$\tilde{\delta}_x \equiv \begin{cases} -1, & 2nw \le x < (2n+1)w \\ 1, & (2n+1)w \le x < 2(n+1)w \end{cases} \tag{14}$$

where n is an integer and h_i is the strength of the interaction between the walls and the respective i segments. Moreover, w is the width of an individual stripe, and δ_{ab} is the Kronecker delta. The pattern on the lower surface thus corresponds to long stripes parallel to the y-direction. Notice that ϕ_i can be expressed in terms of the order parameter Ψ, i.e., $\phi_A = f + \Psi/2$ and $\phi_B = 1 - f - \Psi/2$.

Numerical Cell Dynamics Simulation. The numerical scheme introduced to implement the dynamic model described so far is based on the definition of the fields in a cubic lattice, together with an appropriate discretization of the Laplacian in eq 4.[89] We propose

$$\Psi(i, j, k; t+1) = \Psi(i, j, k; t) - \{\langle\langle \Gamma(i, j, k; t)\rangle\rangle - \Gamma(i, j, k; t) + B\Psi(i, j, k; t)\} \tag{15}$$

Here (i,j,k) stands for the set of indices of a given grid point on the lattice, and $\langle\langle\Gamma\rangle\rangle - \Gamma$ stands for a discrete Laplacian defined by[68,90]

$$\langle\langle\Psi\rangle\rangle = \frac{6}{80}\sum_{NN}\Psi + \frac{3}{80}\sum_{NNN}\Psi + \frac{1}{80}\sum_{NNNN}\Psi \tag{16}$$

where NN denotes nearest neighbors, NNN next-nearest neighbors, and $NNNN$ next-next-nearest neighbors of a point (i,j,k).

The function Γ is defined as

$$\Gamma(i, j, k; t) = g(\Psi(i, j, k; t)) - \Psi(i, j, k; t) + D[\langle\langle\Psi(i, j, k; t)\rangle\rangle - \Psi(i, j, k; t)] - s_i(z) \tag{17}$$

Finally, the so-called map function $g(\Psi(i,j,k;t))$ is directly related to the functional derivative of H given in eq 8. For our particular system it reads[84,91]

$$g(\Psi(i, j, k; t)) = [1 + \tau - A(1-2f)^2]\Psi - v(1-2f)\Psi^2 - u\Psi^3 \tag{18}$$

Free Energy Functional on the Lattice. The transition from the continuous space to the lattice introduces necessary prescriptions for the evaluation of the Laplacian and the nonlocal contribution appearing in the definition of the free energy functional, defined in continuous space in eq 7. As a consequence, we cannot construct the corresponding free energy functional model on the lattice by the direct discretization of the right-hand side of eq 7, expecting that this model has the required properties for the discrete field, namely, that the dynamics implemented in eq 15 progresses monotonously lowering the value of the free energy functional to its minimum at equilibrium. The discrete counterpart of the functional derivative of the free energy functional should be compatible with the second term on the right-hand side of eq 15, after the discrete Laplacian is taken, according to eqs 3 and 4.

Let $F[\Psi(i,j,k)]$ be the free-energy functional of the field $\Psi(i,j,k)$ defined on the lattice. The counterpart of the functional differentiation on the lattice at a given point (i,j,k) is simply the partial derivative with respect to the field at the given point. Hence, the chemical potential in the lattice reads

$$\mu(i, j, k) = \frac{\partial F}{\partial \Psi(i, j, k)} \tag{19}$$

Accordingly, the dynamic equation (15) can be written as

$$\Psi(i, j, k; t+1) = \Psi(i, j, k; t) + \langle\langle\mu(i, j, k)\rangle\rangle - \mu(i, j, k) \tag{20}$$

Therefore, the key point is to provide a discrete free energy whose functional derivative on the lattice, eq 19, gives a chemical potential field such that eq 20 is identical to eq 15. We thus propose

$$F[\Psi(i, j, k)] = \sum_{i,j,k}\left(H[\Psi] - \frac{D}{2}\Psi[\langle\langle\Psi\rangle\rangle - \Psi] + \frac{B}{2}\mu^{(lr)}\Psi + s_A\left[\frac{\Psi}{2} + f\right]\right) \tag{21}$$

where both Ψ and $\mu^{(lr)}$ on the right-hand side of eq 21 are calculated at the grid point (i,j,k). Furthermore, $\mu^{(lr)}$ is the solution of the algebraic set of equations defined from the relation

$$\langle\langle\mu^{(lr)}(i, j, k)\rangle\rangle - \mu^{(lr)}(i, j, k) = -\Psi_{i,j,k} \tag{22}$$

which corresponds to the discrete Laplacian of the long-range term equated to the thermodynamic force used on eq 15, according to eq 20. One can iteratively solve the set of eqs 22 and substitute the field as well as the resulting $\mu^{(lr)}$ in eq 21 to obtain the numerical value of the free energy functional for a given field Ψ defined in the lattice.

The obtained free-energy functional on the lattice is thus compatible with the implemented dynamic equation and therefore has the desired properties. The value of the free energy at the final state of the simulation is be used to compare the relative stability of the obtained structures.

3. RESULTS AND DISCUSSION

Model System. In this study we consider a sphere-forming diblock copolymer melt. The CDS parameters are $f = 0.4$, $u = 0.38$, $v = 2.3$, $B = 0.01$, $D = 0.5$, $A = 1.5$, and $\tau = 0.2$, which are known to produce spherical domains.[92,93] The morphological characteristics of such spherical domains are the spacing between spheres $d \simeq 11$ and their average diameter $\phi \simeq 7.8$ in units of lattice spacings a_0 (see Figure 1). These parameters are taken from Pinna et al.[93] and correspond to the morphology of a monolayer of spheres formed in a slit with homogeneous surfaces selectively attracting the minority A-block.

Our system is BCP confined in a slit of hard walls. The lower surface is decorated with a mask of stripes with different affinity to the blocks of the BCP, i.e., different values of s_i in eq 7. In particular, we have chosen $h_A = 0.1$ and $h_B = -0.1$ according to

DOI: 10.1021/acs.macromol.5b02314
Macromolecules XXXX, XXX, XXX−XXX

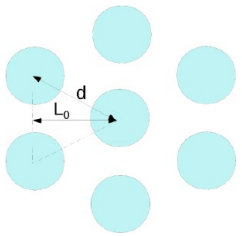

Figure 1. Sphere-froming BCP in a planar hexagonal cell with the characteristic dimensions. The natural lateral period for the hexagonal forming system[93] is $L_0 \simeq 9.5$ ($L_0 = \sqrt{3}/2d$).

eqs 13 and 14. The upper surface of the slit is neutral ($s_i = 0$ for all blocks i). These solid walls are located at the position $z = 1$ for the bottom surface and $z = L_z$ for the top surface, as shown in Figure 2a. The pattern on the bottom surface corresponds to

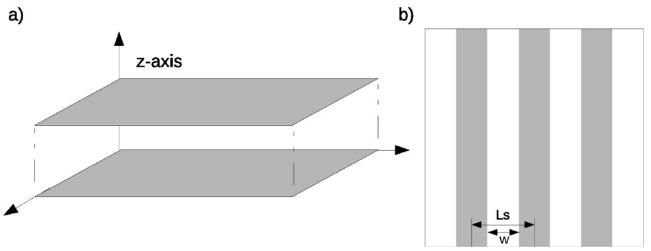

Figure 2. (a) Setup and (b) mask.

a set of alternating parallel stripes along the y-direction, whose width is $w = L_S/2$, as depicted in Figure 2b. Thus, the distance between equal stripes (or band periodicity) is L_S. We have verified that the morphology of the patterns observed is rather insensitive to the attraction energy h if the latter is kept within the range from 0.1 to 0.4. Hence, for convenience, we have chosen $h = 0.1$ in all the simulations. Periodic boundary conditions (PBC) are set for the x- and y-directions. The boundary condition of zero flux of Ψ at the hard surfaces implies that the gradient of the chemical potential eq 3 vanishes at the interfaces.[87] Numerically, such a condition is fulfilled by extending the field inside the wall and demanding $\Psi(x,y,z = 0) = \Psi(x,y,z = 1)$ and $\Psi(x,y,z = L_z + 1) = \Psi(x,y,z = L_z)$, where $z = 0$ and $z = L_z + 1$ are the coordinates of the extended layers.[88]

We have considered systems of lateral size $L_x = L_y = 120 \simeq 11d$ with different thicknesses L_z ranging from 6 to 56 grid spacings (from $0.5d$ to $5d$, approximately). In every case, three different band periodicities of $L_S = 8$, 10, and 12 are studied. These values guarantee that L_S is commensurate with L_x, so that L_x/L_S is an integer, to comply with the periodic boundary conditions. In the experimental work of Park et al.,[10] the authors have chosen a band periodicity $L_S \simeq L_0$, where L_0 is defined in Figure 1, with $L_0 = \sqrt{3}/2d \simeq 0.86d$, which corresponds approximately to 9.5 lattice spacings. Variations $L_S < L_0$ and $L_S > L_0$ were also studied in this last reference. Our choice of the values of L_S in the simulation aims at reproducing these experimental situations.

The equilibrium structures have been computationally determined by the dynamic evolution of the CDS. The simulation starts from an homogeneous state on which we have superimposed a random perturbation to the order parameter field $\Psi = \pm 0.5$ at every grid point. The deterministic dynamics given in eq 15 progresses until a final state, where no variation in the order parameter field is observed. In general, the evolution leads to spherical domains characterized by values of the field $\Psi \simeq \Psi^-$, where Ψ^- is the negative minimum of H in eq 8. This dynamics corresponds to a quench of the system at a given temperature below the critical temperature, which in our case is $\tau' = -0.14$ (for a qualitative analysis of the system, see the Supporting Information). The progress of the quench dynamics starts with a fast process, dominated by spinodal decomposition, in which the domains grow from the local initial inhomogeneities. Then, it follows a much slower process of rearrangements of the domains in space and size. While the former process takes between 1000 and 10 000 time steps, the latter takes of the order of 10^7 time steps or longer.

The approach to equilibrium can be monitored through the free energy of the system given by eq 21. However, we cannot guarantee that the final structures, even after our long simulation runs, correspond to true equilibrium arrangements, since they could also be metastable states caused by local free-energy minima. To overcome metastable states, we have added a random noise[86,94] to the evolution equation, eq 15, according to

$$\Psi(i,j,k;t+1) = \Psi(i,j,k;t) - \{\langle\langle\Gamma(i,j,k;t)\rangle\rangle - \Gamma(i,j,k;t) + B\Psi(i,j,k;t) - \zeta\} \quad (23)$$

where ζ is a white noise process with a given amplitude. As we have discussed in the previous section, the fluctuation−dissipation theorem does not apply here since this term is a computational artifact and is not intended to reproduce thermal noise. We recall that the physical dynamics is deterministic with the temperature embedded in the parameter τ', which is the control parameter of the phase separation.[79] Hence, there is no inherent physical temperature scale in the amplitude of ζ as we use it along this article. In all cases, the final configuration is obtained after setting $\zeta = 0$ for at least 100 000 time steps before the end.

We employ a second dynamic procedure based on annealing. As before, the initial state is a homogeneous field with analogous superimposed random inhomogeneities. Here, instead, the value of τ' is linearly lowered with time. We have chosen the system to decrease from $\tau' = 0$ to the final $\tau' = -0.14$ in a given lapse of the order of the total time. When performing the annealing, the free energy does not significantly change until a threshold, which varies with the system, is reached. Then, the free energy drops near the final equilibrium value. Noise is also added to the dynamic evolution and switched off during the last 100 000 time steps.

The initial stages of two representative free energy trajectories for quenching as well as annealing without added noise are shown in Figure 3. In this example the sudden change of slope in the annealing occurs at around $t \simeq 20\,000$, corresponding to $\tau' \simeq -0.11$. The dynamic routes to equilibrium are very different, depending on whether quenching or annealing is chosen, meaning that the system evolves through different intermediate structures depending on the route. In Figure 4 we show a sequence of intermediate structures from the same initial state and leading to the same final state, for both quenching and annealing. The final states are compared with regard to their free energy to elucidate which is more stable. In the figures, only A-rich regions are shown while the empty space correspond to B-rich regions.

Without the addition of the noise, annealing would invariably produce metastable cylinders even close to the final temperature $\tau' = -0.14$. The noise, however, moves the system toward

DOI: 10.1021/acs.macromol.5b02314
Macromolecules XXXX, XXX, XXX−XXX

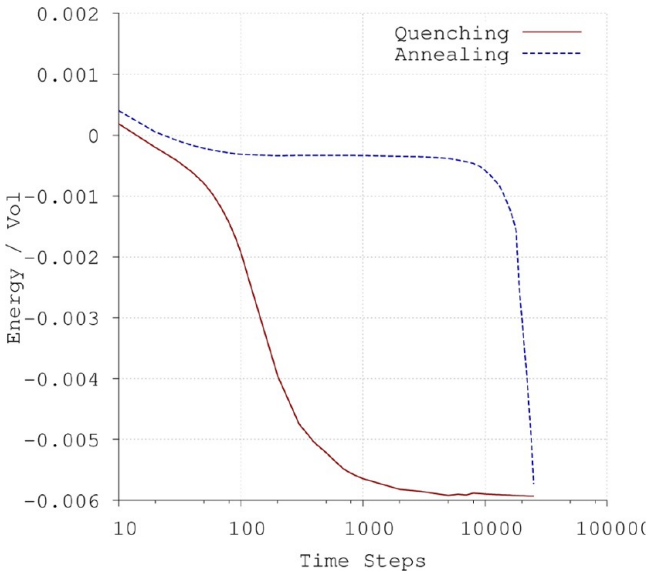

Figure 3. Initial steps of the free energy evolution for the quenching and the annealing processes without added noise.

lower energy configurations consisting of ordered arrangements of spheres. Annealing is particularly useful for frustrated situations where quenching often leads to a final state consisting of a disordered array of spheres. The evaluation of the free energy of the system permits us to discriminate the more stable configuration when the two routes produce different results for the same system.

Slits $L_z \leq d$. Let us consider narrow slits whose thickness is of the order of or smaller than the BCP characteristic domain separation d, which is proportional to the polymer chain length,[66] $d \sim N^{2/3}$ (see also the Supporting Information). The analysis of this particular case permits us to check the validity of the model for the study of BCP systems under confinement.

Park et al.[10] experimentally studied P(S-*b*-MMA) on chemically patterned surfaces giving spherical domains with $\phi \simeq 26.5$ nm and $d \simeq 65.2$ nm. Their experimental systems consist of a slit with different thicknesses and an area of $30 \times 400\ \mu m^2$. On the bottom surface the system presents a striped (line-and-space) pattern, with a periodicity (band periodicity) ranging from $L_S = 50.0$ to 60.0 nm. The systems with $L_z = 25$ nm, which correspond to a slit thickness significantly smaller than d, produce scattered domains with no order and a wetting layer for each block on the corresponding attractive bands. If we base our comparison between experimental and simulation results on d, these systems would correspond to $L_z \simeq 5$ and L_S from 8 to 10 grid spacings in our simulation. As seen in Figures 5a and 5b, the structures predicted by our simulation for $L_z = 6$ and $L_S = 8$ and 10, respectively, agree very well with the experimental results shown in Figure 2 of Park et al.[10] Hence, the CDS can be compared with physical systems taking the characteristic distance d as a reference.

Moreover, this good agreement in a narrow slit indicates that the free-energy functional given in eq 7 is able to reproduce almost quantitatively the experimental results. The kernel of the long-range contribution in eq 7 should contain an explicit dependence on the distance z to the hard walls when $z < d$. However, in view of the comparison with experimental results, the effects of such contribution are not relevant, and therefore one can use the isotropic propagator $G(\mathbf{r})$ in all cases, as a good approximation.

We next address the case of a thin slit $L_z = 8 \simeq 0.7d$ to analyze the effects of the width of the stripes on the structure of the BCP system. For comparison purposes, let us first consider a nonpatterned homogeneous lower surface for which the boundary conditions are set to be the same as in the upper surface. In general, these neutral boundary conditions favor the formation of semispheres (spherical caps) in contact with the hard walls if no other constraints are applied. Effectively, spherical caps at the surfaces permit the BCP chains close to it to lay unstretched parallel to the wall. Spheres tangent to the hard wall are not entropically favored due to the fact that polymer blocks in the corona shell are forced to squeeze

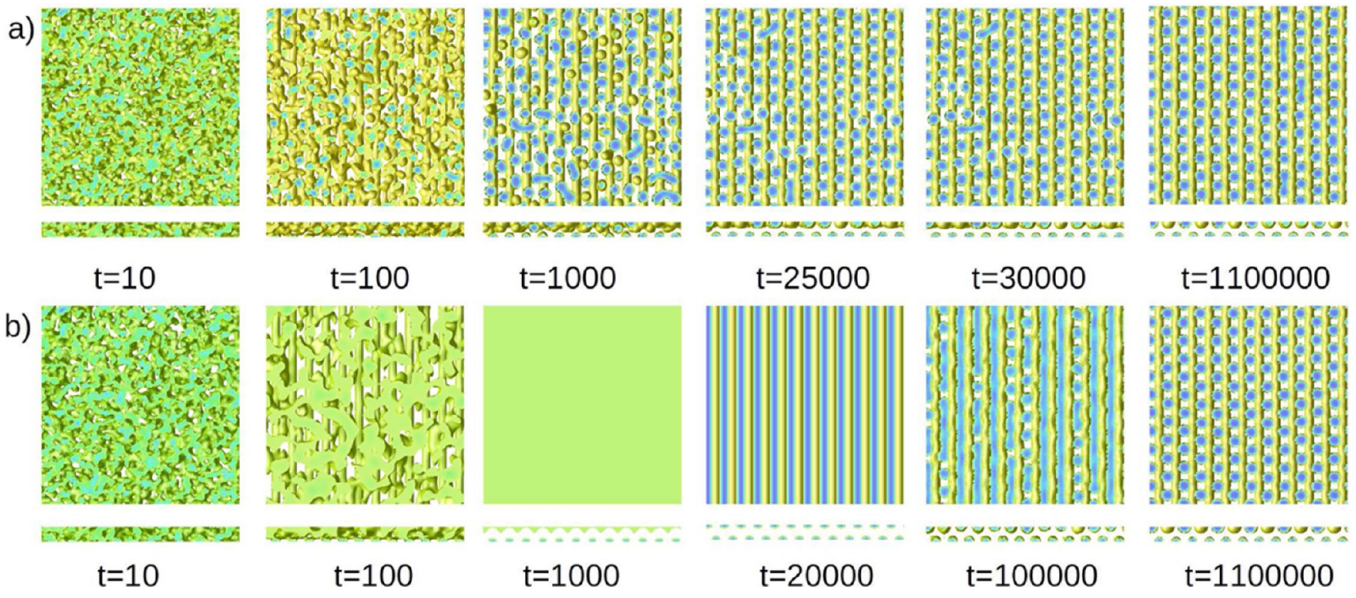

Figure 4. Evolution of the configurations of a sphere-forming BCP confined by solid surfaces: (a) quenching and (b) annealing. Box size $L_x = L_y = 120$, $L_z = 10$. The square frames show the top view, while the rectangles are side views in the y-direction, along which the stripes with $L_S = 10$ lie. The scale of color ranges from light, $\Psi^+ = 0.25$, to dark, $\Psi^- = -1.46$, where $\Psi^\pm$ are the minima of H.

DOI: 10.1021/acs.macromol.5b02314
Macromolecules XXXX, XXX, XXX−XXX

between the sphere and the wall. This type of confinement of the BCP system therefore produces frustrated situations.

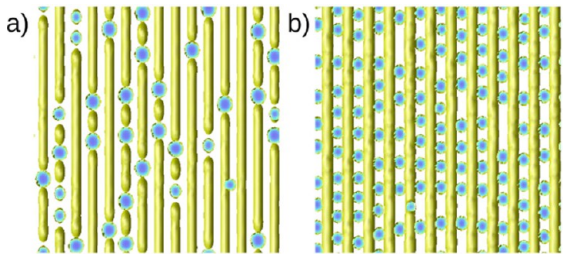

Figure 5. CDS simulations of sphere-forming BCP confined by solid surfaces. Bottom surface chemically activated with stripes attractive to A block and B block alternately and top surface neutral. Box size $L_x = L_y = 120$, $L_z = 6$. (a) Top view of the morphology with stripes whose spacing is $L_S = 8$ and (b) $L_S = 10$.

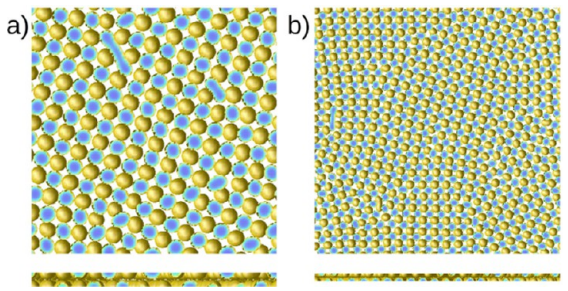

Figure 6. CDS simulations of sphere-forming BCP confined by two homogeneous and neutral solid surfaces. Top and side view of the morphology. Box size: (a) $L_x = L_y = 120$, $L_z = 8$ and (b) $L_x = L_y = 240$, $L_z = 8$.

From Figure 6a we observe that two layers of semispheres are formed attached to both the upper and lower surfaces. These semispheres have a tendency to arrange in squares although the figure does not show a clear long-range order. This configuration, however, may not correspond to an equilibrium system. The defects are a signature of a rather degenerated free-energy landscape, since the model we use does not account for thermal fluctuations. The explicit consideration of the noise in this kind of situation could significantly change the phase diagram and the nature of the order−disorder transitions.[69,95,96] Figure 6b shows a system 4 times the size of the one of Figure 6a, after the same evolution time and from analogous initial conditions. While isolated dislocations are visible in the smaller system, the larger system shows also grain boundaries which become observable due to the less stringent effect of PBC in the long-range order for the bigger box.

It may seem surprising that the dominating structure is square instead of hexagonal, since hard walls tend to favor compact arrangements of hard spheres at their immediate vicinity. However, one should bear in mind that the slit thickness L_z is smaller than $d\sqrt{2/3} \simeq 9$, which is the distance between layers of spheres in hexagonal packing. Hence, the system chooses to form a square structure that permits the two layers of spheres to interpenetrate with regularity, in a way that a compact hexagonal phase cannot. Notice that the distance between (100) planes of a BCC, whose distance between the central sphere and one at the vertex of the cell is approximately d, is of the order of $d/\sqrt{3} \simeq 6.3$, which is smaller than the actual $L_z = 8$. Therefore, the square structure is the result of the need of the system to accommodate two close layers of spherical caps forced by the slit thickness.

The presence of the pattern of chemical stripes in the lower surface for the same system $L_z = 8$ has an additional ordering effect. However, the impact of the pattern on the final configuration of spheres depends upon the commensurability of the periodicity of the stripes L_S and the characteristic lengths of the physical system. Let us first consider a pattern with band periodicity $L_S = 8 < L_0$, which is approximately equal to the sphere diameter but smaller than the natural distance between spheres, $d \simeq 11$. The structure with lowest energy in this case is given in Figure 7a. On the bottom surface semicylindrical

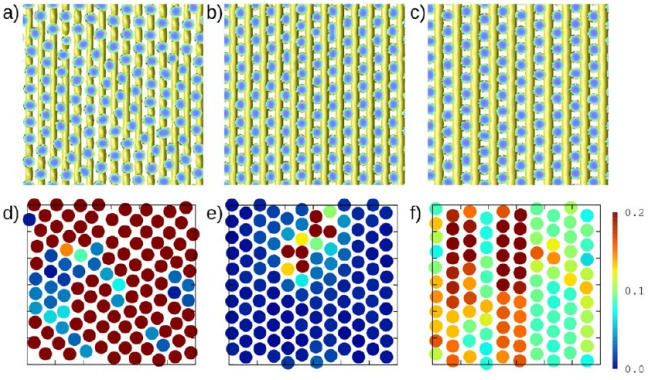

Figure 7. CDS simulations of sphere-forming BCP confined by solid surfaces. Bottom surface chemically activated with stripes attractive to A block and B block alternately and top surface neutral. Box size: $L_x = L_y = 120$, $L_z = 8$. (a) Top view of the morphology with stripes whose spacing is $L_S = 8$, (b) $L_S = 10$, and (c) $L_S = 12$. Euclidean distance of the local environments of each spherical domain to the HEX pattern, using a scale of colors. Dark blue indicates a small distance and dark red indicates a large distance to the HEX pattern: (d) $L_S = 8$, (e) $L_S = 10$, and (f) $L_S = 12$.

domains, wetting the A-attracting bands, form. Moreover, a layer of semispheres, attached to the upper surface, also appear. Unlike the nonpatterned case, the bottom layer cannot freely match the structure formed on the upper surface and satisfy the periodicity introduced by the bands. This difference in the periodicity is known as *surface reconstruction*. Therefore, the addition of the bands causes a change in the *native* arrangement, as shown in Figure 6, yielding a closer packing of spherical domains than in the nonpatterned case. The structure, however, has many defects, and in some regions square arrangements are still observed. That is mainly because of the mismatch between the horizontal periodicity of the domains in the upper layer, $L_0 \simeq 9.5$, and the band periodicity, $L_S = 8$. Simulations of larger system sizes, together with 2-D Fourier transform of the patterns, confirm that there is no long-range order.

From the $L_S = 8$ case we see that the system has a rather degenerate free-energy landscape. Effectively, in Figure 8a we show the regular structure obtained from the annealing route for the same system. The value of the free-energy for the latter is, however, slightly larger than for the structure in Figure 7a, obtained from quenching. The bottom view of the system, shown in Figure 8b, reveals that the cylinders are broken at the position of the semispheres.

For the case $L_S = 10 \simeq L_0$ we match the commensurability between the natural distance for a 2-D HEX structure and the

DOI: 10.1021/acs.macromol.5b02314
Macromolecules XXXX, XXX, XXX−XXX

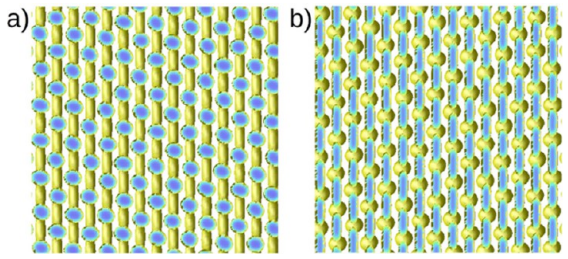

Figure 8. Sphere-forming BCP confined between a homogeneous and neutral surface on the top and a patterned surface on the bottom with chemically active stripes with a separation $L_S = 8$. State obtained from annealing. (a) Top view and (b) bottom view. Box size: $L_x = L_y = 120$, $L_z = 8$.

periodicity of the stripes, namely $L_S \simeq L_0$, according to Figure 1. In Figure 7b we observe that in the upper layer an expected regular hexagonal pattern of spherical caps lying in the valley between half-cylinders appears. Finally, the case $L_S = 12 > L_0$ yields a regular structure with the spherical caps of the upper surface also lying in the corresponding valleys. However, the structure is forced to comply with the periodicity imposed by the stripes in the x-direction. The structure is then slightly stretched yielding a distance between half-spheres belonging to parallel rows approximately $\sqrt{L_S^2 + d^2/4} \simeq 13.2 > d$. In turn, the distance between spheres in the same row is slightly smaller than d, and no surface reconstruction occur. The resulting structure is then similar to the hexagonal, as seen in Figure 7c. In Figure 7d–f we show for every case the obtained Euclidean distances (cf. Supporting Information) from the local environments of each spherical domain to the one corresponding to a 2-D HEX pattern. For a perfect hexagonal ordering, this distance would be 0. For the three systems under scrutiny we find that for $L_S = 8$ only some spherical domains are surrounded by a clear hexagonal pattern; for $L_S = 10$, Figure 7e indicates that the 2-D HEX structure is indeed dominant, except for a few defects; finally, when $L_S = 12$, the system shows a clear deviation from a hexagonal symmetry, although it is not evident to the eye. We have further checked, for this latter $L_S = 12$ system, that the Euclidean distance to a (110) plane of a BCC pattern is larger than to the 2-D HEX. Hence, the new structure cannot be considered as a precursor of a bulk BCC.

The next case studied is $L_z = 10 \simeq 0.9d$. First, the system $L_S = 8 < L_0$ in Figure 9a approximately corresponds to the experimental system with $L_z = 57$ nm and $L_S = 50$ nm in Park et al.,[10] where we use $d = 11 \approx 65.2$ nm for comparison, as before. Here, the regions with squares, observed for a thickness of $L_z = 8$, have disappeared. The matching between the patterns in the upper and lower layer for this band periodicity is less stringent for a thickness of the order of the natural distance between spherical domains. Then hexagonal structures are observed, although no long-range order exists, in agreement with the experimental results[10] (see Figure 4 of this last reference). Our CDS data thus confirm that such narrow bands are not capable of guiding the assembled BCP spherical domains toward a regular pattern with long-range order. Again, surface reconstruction occurs as an undesirable result causing the mismatch between the natural spacing of the spheres and the band periodicity.

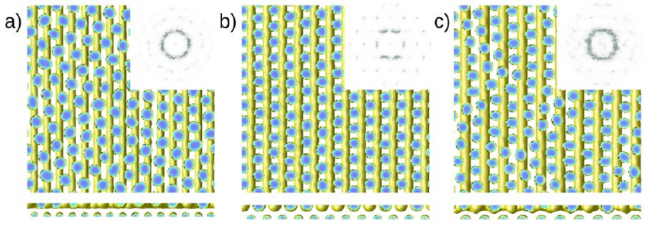

Figure 9. CDS simulations of sphere-forming BCP confined by solid surfaces. Bottom surface chemically activated with stripes attractive to A block and B block alternately and top surface neutral. Top and side view of the morphology when the box size is $L_x = L_y = 120$, $L_z = 10$ and the stripes have a spacing of (a) $L_S = 8$, (b) $L_S = 10$, and (c) $L_S = 12$. The insets show the corresponding 2-D fast Fourier transform.

Second, the system with $L_S = 10 \simeq L_0$ (Figure 9b) produces a well-ordered upper layer of spherical caps. These results are in perfect agreement with the corresponding system $L_z = 57$ nm and $L_S = 60$ nm described in Figure 4 from Park et al.[10] As compared with the previous cases, here the system prefers to form a 2-D HEX layer of spherical caps which perfectly matches the periodicity of the stripes of the bottom layer. Figure 10 shows the system $L_S = 10$ cropped at $z = 4$. One can distinguish knurled cylindrical domains which also reproduce experimental observations.[10]

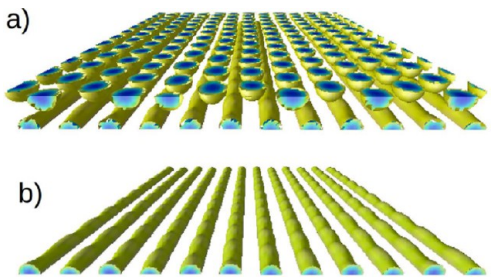

Figure 10. 3-D view of system with $L_S = 10$ at different heights: (a) at $L_z = 4$; (b) at $L_z = 10$.

Beyond the band periodicity experimentally studied we have also analyzed, in the third place, the case $L_S = 12 > L_0$ that would physically correspond to a band periodicity of 71 nm. Here, this band periodicity matches approximately the length of the edge of a BCC cell, $2d/\sqrt{3} \simeq 12.7$, where the shortest distance apex center is d. However, for this particular slit thickness the bands are not capable of producing a (100) BCC plane on the upper surface, but rather a local HEX-like structure with no long-range order. The comparison of this latter case with $L_z = 8$ (cf. Figure 9c) suggests that the periodicity in the x-direction is not uniquely imposed by the band spacing, unlike suggested elsewhere.[10]

It is particularly interesting that a slight increase of the slit thickness from $L_z = 10$ to 12 for the same $L_S = 12$ produces a completely different scenario, which is shown in Figure 11. The pattern has long-range order and is rectangular, slightly stretched in the y-direction. The new pattern contains an additional layer of complete spheres between the upper and lower layers of half-domains. Then the periodicity of the arrangements of spheres in the x-direction perfectly matches the band spacing. The dimensions of the unit cell are estimated as being of 12 lattice spacings in the x-direction and of 13.3 in the y-direction, parallel to the stripes. The unit cell is then a body-centered orthorhombic (BCO).

Slit $L_z = 14$. We also investigated the morphology of systems contained in a slit with thickness $L_z = 14 \simeq 1.3d$. The

DOI: 10.1021/acs.macromol.5b02314
Macromolecules XXXX, XXX, XXX–XXX

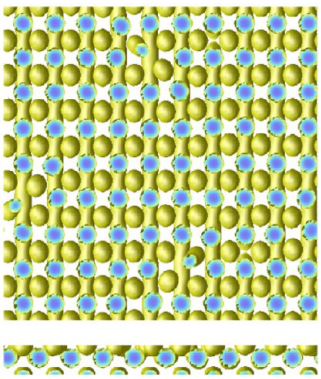

Figure 11. CDS simulations of sphere-forming BCP confined by solid surfaces. Bottom surface chemically activated with stripes attractive to A block and B block alternately and top surface neutral. Top and side view of the morphology when the box size is $L_x = L_y = 120$, $L_z = 12$ and the stripes have a spacing of $L_S = 12$.

spherical caps forming 2-D HEX pattern of the previous $L_z = 10$ case are transformed in a layer of complete spheres almost tangent to the hard wall, which is entropically unfavorable. The system is therefore frustrated if 2-D HEX layers are to be formed in a slit where L_z is slightly larger than d.

The first case $L_S = 8 < L_0$ produces complete tangent spheres locally ordered in hexagonal arrangements in addition of the half-cylinders formed on the lower hard wall, according to Figure 12a. Some of the domains in the upper layer, however,

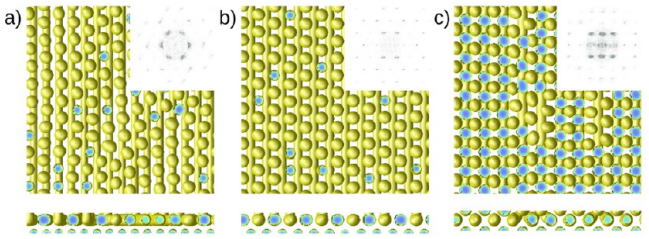

Figure 12. CDS simulations of sphere-forming BCP confined by solid surfaces. Bottom surface chemically activated with stripes attractive to A block and B block alternately and top surface neutral. Top and side view of the morphology when the box size is $L_x = L_y = 120$, $L_z = 14$ and the stripes have a spacing of (a) $L_S = 8$, (b) $L_S = 10$, and (c) $L_S = 12$. The insets show the corresponding 2-D fast Fourier transform.

are deformed into structures that vaguely resemble eggplants, due to the aforementioned frustration. The overall behavior is very similar to the previously studied case $L_z = 10$ for the same band periodicity. We observe here again surface reconstruction with lost of long-range order in larger systems (not shown). Hence, bands cannot guide the assembly of the upper layer of spheres.

As expected, for the case $L_S = 10$ there is a clear effect of the commensurability, since $L_S \simeq L_0$, in view of Figure 12b. The arrangement obtained corresponds to upper layer of complete spheres laying tangent to the hard wall, with a long-range 2-D HEX symmetry. Some defects in the form of eggplant domains are also present, and the distribution of domains in the upper layer is similar to the previous cases studied for this band periodicity. Our simulation results are in agreement with the patterns encountered in the system $L_S = 60$ nm in a slit $L_z = 70$ nm,[10] although we find a slightly better long-range ordered structures.

Finally, the most interesting situation occurs for the band periodicity to $L_S = 12 > L_0$. Figure 12c shows an extra layer of domains that are formed in contact with the upper wall, as already encountered for the case $L_z = 12$ with the same band spacing. The order is long-range and corresponds to BCO with the (100) plane parallel to the hard surfaces. This is a clear example of the interplay of both the band periodicity and the slit thickness to favor a given 3-D cell. In this particular case, a BCO is favored due to the fact that the slit thickness is close to $2d/\sqrt{3} \simeq 12.7$ and that the band periodicity is precisely close to this same length.

Thicker Slits. In the previously analyzed cases we have verified that the sphere-forming BCP are very sensitive to the band periodicity, which should be commensurate with the characteristics distance d of the BCP in order to produce neat ordered arrangements. We have seen that the vertical confinement also plays an important role in determining the final structure. In this section we attempt to rationalize these two ideas for systems where many layers of spheres can form.

If the system forms n layers of complete spheres stacked in a 3-D HEX packing, then the appropriate slit thickness should be approximately given by

$$L_z(\mathrm{HEX}_1) \equiv (n+1)d\sqrt{\frac{2}{3}} \tag{24}$$

We have considered that the distance between neighboring spheres is approximately d and that the distance between layers parallel to the walls is $d\sqrt{2/3}$, corresponding to a 3-D HEX packing of hard spheres of a diameter d. An additional layer of spherical caps forms in contact with the top surface. The distance between the half-cylinders at the lower surface and the first layer of spheres has been assimilated to the distance between neighboring planes of spheres.

In the same way, if the system is prone to form a BCC unit cell with its base parallel to the hard walls, the appropriate slit thickness should be approximately given by

$$L_z(\mathrm{BCC}) \equiv (n+1)\frac{d}{\sqrt{3}} \tag{25}$$

Here, the distance between layers is $d/\sqrt{3}$, as it corresponds to (100) planes of a BCC. Again, a layer of spherical caps is considered to form on the upper wall while the shortest distance between neighboring spheres is assumed to be approximately d.

Slit thicknesses laying off these periodicities impose some degree of frustration in the system, which may produce slightly stretched or compressed unit cells, or the formation of entropically unfavorable tangent spheres near the upper wall. In particular, a slit thickness given by

$$L_z(\mathrm{HEX}_2) \equiv \left(n+\frac{1}{2}\right)d\sqrt{\frac{2}{3}} \tag{26}$$

with 3-D HEX packing would produce such a frustrated system with tangent spheres. Equations 24−26 cannot be taken as exact by different reasons, the most important being that the system can modify its characteristic length under constraint to a given extent. These expressions only give a rough estimate of what one can expect.

In the first place, let us study the structures obtained for the three band periodicities $L_S = 8$, 10, and 12 for systems with slit thicknesses $L_z = 20$, 24, and 36 (corresponding to $1.8d$, $2.2d$,

DOI: 10.1021/acs.macromol.5b02314
Macromolecules XXXX, XXX, XXX−XXX

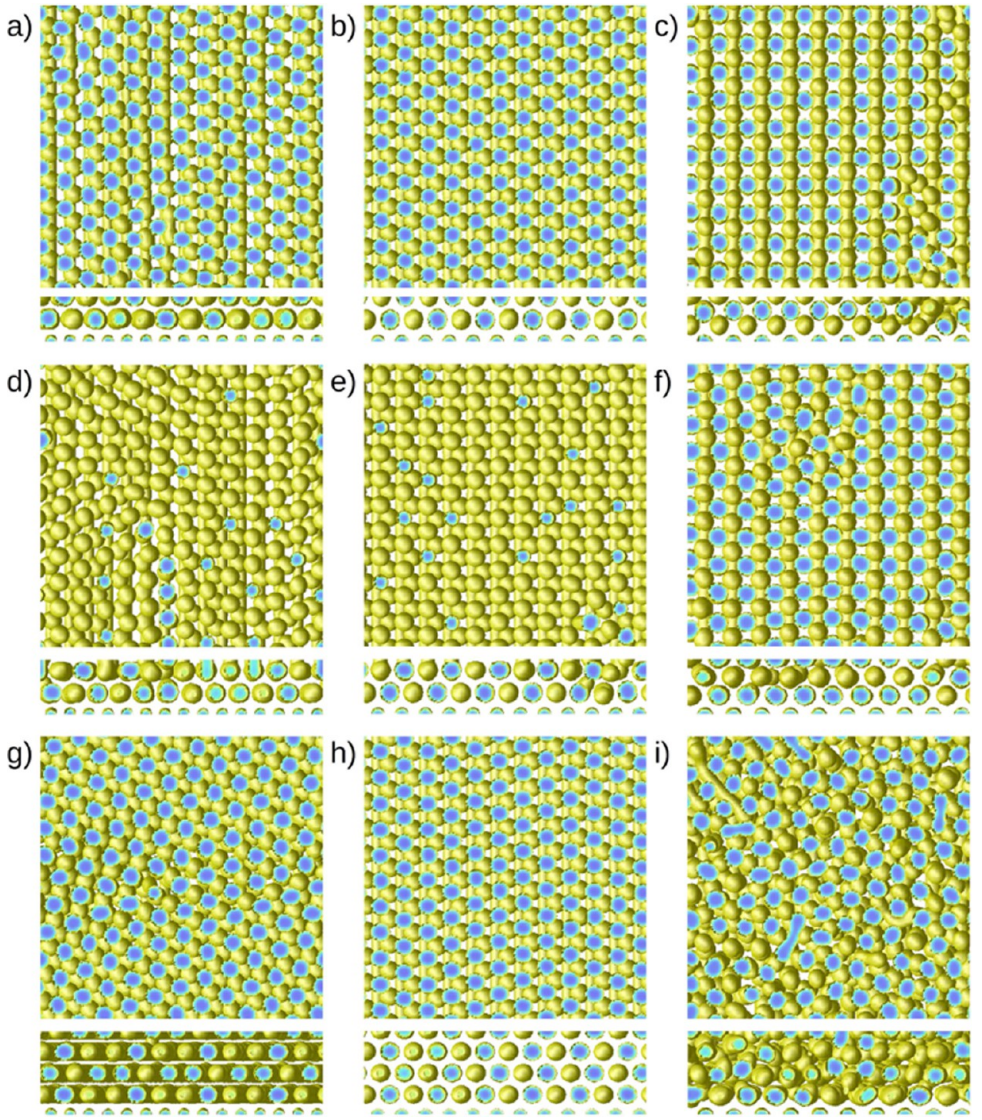

Figure 13. CDS simulations of sphere-forming BCP confined by solid surfaces. Bottom surface chemically activated with stripes attractive to A block and B block alternately and top surface neutral. Top and side view of the morphology when the box size is $L_x = L_y = 120$, $L_z = 20$ and the stripes have a spacing of (a) $L_S = 8$, (b) $L_S = 10$, and (c) $L_S = 12$. Top view for a box size $L_x = L_y = 120$, $L_z = 24$ and lattice spacing of the stripes (d) $L_S = 8$, (e) $L_S = 10$, and (f) $L_S = 12$. Top view for a box size $L_x = L_y = 120$, $L_z = 36$ and lattice spacing of the stripes (g) $L_S = 8$, (h) $L_S = 10$, and (i) $L_S = 12$.

and 3.3d, respectively). The particular thicknesses chosen for the first and the third cases correspond to values that approximately comply with eq 24, with $n = 1$ and $n = 3$. The second thickness roughly corresponds to eq 26 with $n = 2$. In Figure 13 we show the structures obtained for the mentioned periodicities and thicknesses.

First, let us center our attention to the case of a bandwidth $L_S = 8 < L_0$. Here, the structure is dominated by the geometrical confinement. Figures 13a,g show a 2-D hexagonal pattern in the upper layer, with spherical caps. Figure 13d shows the same structure but for tangent spheres. The mismatch between the bandwidth and the 2-D HEX pattern is seen in the lateral views of the systems in the same set of figures. Although the system shows local order, many defects in the structure are visible for the three thicknesses. Surface reconstruction is also visible.

Second, Figures 13b,e,h correspond to a band periodicity $L_S = 10 \simeq L_0$, compatible with the formation of a 2-D hexagonal pattern in the first layer of spheres (bottom up). For the three thicknesses, we observe long-range order in all the layers. From $L_z = 36$ we further see that the three layers of complete spheres together with the upper layer of spherical caps are packed in a clear 3-D HEX, with a distance between layers of spheres $\delta \simeq 9 \simeq d\sqrt{2/3}$. Effectively, from the top view of Figure 13h we see that the top layer of spherical caps and the second layer bottom up are on top of each other, as it corresponds to this 3-D HEX structure (see also the lateral view). The calculation of the Euclidean distance at each layer of spheres also reveals that the local structures are indeed hexagons (Euclidean distances to the reference pattern are of the order of 10^{-2}). The case $L_z = 24$ corresponds to tangent spheres. The system keeps the overall 3-D HEX configuration despite the fact that tangent spheres are entropically less favored. It is worth remarking that the distance between planes for this latter case is $\delta \simeq 9.6$ instead of 9, slightly stretched with respect to a 3-D HEX packing.

Third, Figures 13c,f,i correspond to a bandwidth $L_S = 12 > L_0$. With this constraint on the first layer, the system builds a BCO, with a distance between planes $\delta \simeq 6.1$ for the thickness $L_z = 20$, which is very close to the separation between (100)

DOI: 10.1021/acs.macromol.5b02314
Macromolecules XXXX, XXX, XXX−XXX

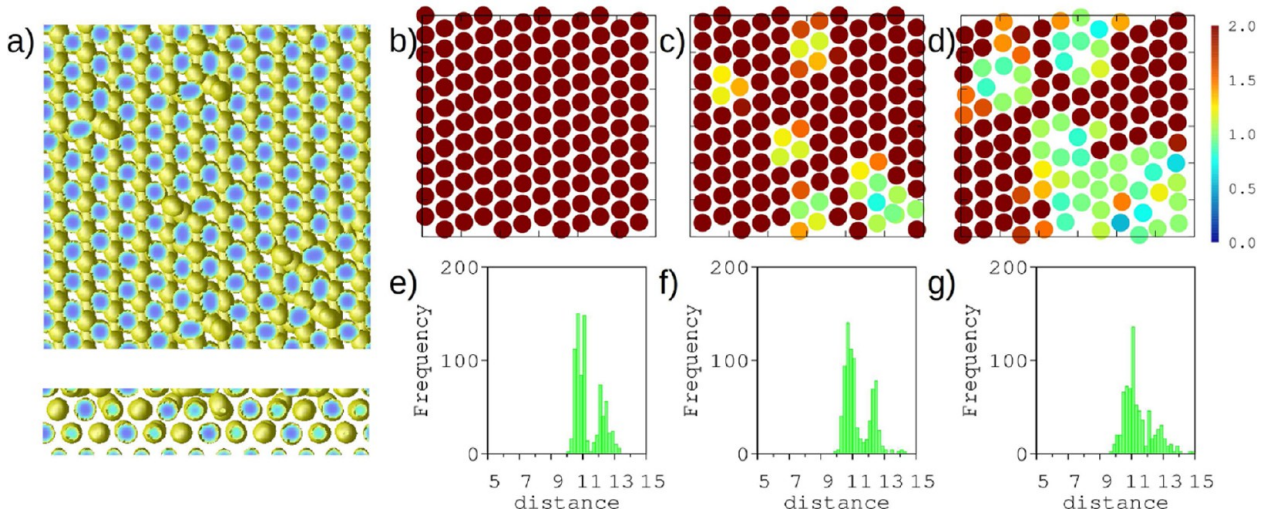

Figure 14. CDS simulations of sphere-forming BCP confined by solid surfaces. Bottom surface chemically activated with stripes attractive to A block and B block alternately and top surface neutral. Box size $L_x = L_y = 120$, $L_z = 26$ and stripes with a spacing of $L_S = 10$. (a) Top and side view of the morphology. Ratio of the Euclidean distance to HEX symmetry and distance to BCC symmetry (d_{HEX}/d_{BCC}); (b) lower layer; (c) middle layer; (d) upper layer. Histogram of the distances of each sphere with its six next-nearest neighbors: (e) lower layer, (f) middle layer, and (g) upper layer.

planes of the BCC lattice, namely, $\delta = d/\sqrt{3} \simeq 6.35$. For the thickness $L_z = 24$, the separation is slightly larger $\delta \simeq 7.7$, as if the system were *stretched* in the z-direction. These two cases present overall long-range order although some defects are visible. However, in Figure 13i we see that the system shows no local order due to the mismatch between the side length of the BCC unit cell and the slit thickness.

Before closing the analysis of the results, several comments are in order. It is well-known that the sphere-forming BCP organize in bulk in BCC structure.[11] The transition between the 2-D hexagonal morphology near a nonpatterned surface and the bulk BCC cell has been studied by Stein et al.[45,97] These authors find a first-order transition at $n \approx 4$ between a 3-D HEX and a face-centered orthorhombic unit cell, which smoothly tends to the bulk BCC as the layer lays farther from the hard surface. Our simulations for $L_S = 10$, which favors the 3-D HEX pattern, thus agree with this experimental finding, particularly when the slit thickness corresponds to eq 24, and therefore, the possible distorting effect of the upper hard wall is minimized. We have found, however, deviations from the expected behavior of 3-D HEX packing in $L_z = 26 \simeq 2.4d$, only slightly thicker than the case $L_z = 24 \simeq 2.2d$, with the same band periodicity $L_S = 10$. Here the slit thickness is close to but smaller than the one given in eq 24 with $n = 2$ and is therefore frustrated. Notice that with respect to the case $L_z = 24$, where the upper layer is tangent to the upper wall, the system $L_z = 26$ forms an additional layer of spherical caps, but not completely developed, as shown in Figure 14a. In Figures 14b–d, we show the ratio between the Euclidean distances of the local structure to both the 2-D HEX and the (110) plane of a BCC. Large values of this ratio indicate that the local environment is closer to the (110) plane of BCC than to the 2-D HEX. Despite the fact that the pattern of the lower surface favors the formation of hexagons, the first layer (bottom up) displays a domain arrangement significantly closer to the (110) BCC than to the HEX. The second layer, however, shows some more disperse spheres surrounded by a HEX environment, while the upper layer of spherical caps is more hexagonal. Obviously, the upper hard wall also imposes a strong confinement constraint that induces a major packing in this layer, favoring the 2-D HEX. However, it is remarkable that the system shows a body-centered structure, close to the bulk BCC, near the lower surface, without passing through intermediate forms of the type of face-centered orthorhombic, as it has been previously reported.[45,97] For completeness, in Figures 14e–g we show the histograms of the distances between every sphere in a given layer to its six closest neighbors. Two peaks are clearly distinguished corresponding to the two characteristic distances of the (110) BCC plane, in the first and second layer. The ratio a_2/a_1 between these two main distances is the order parameter used to describe the transition from HEX to BCC in the aforementioned references. From the histograms we approximately obtain $a_1 \simeq 10.8$ and $a_2 \simeq 12.4$, yielding $a_2/a_1 \simeq 1.15$, which confirms that the layer indeed corresponds to a (110) plane of a BCC. One can then argue that the formation of partial spherical caps on the upper surface *compresses* the structure in the z-direction. Effectively, we measure a distance between planes $\delta \simeq 8$ instead of 9, as would correspond for both the 3-D HEX and the (110) BCC as well. Therefore, the structure is not cubic but rather a body-centered rhombohedron (BCR), instead of the previously observed BCO, due to this compression. It is quite surprising, however, that the surface density of spheres is insensitive to such compression. The case $L_z = 24$ instead displays a clear 3-D HEX packing of the layers. This can be observed from the ratio of the Euclidean distances as well as from the histograms in Figure 15. These behaviors are rather counterintuitive, since the 3-D HEX permits a larger packing density than a BCC for hard spheres and therefore should apparently be preferred in systems under pressure.

A second frustrated system with $L_S = 10$ is the case $L_z = 34 \simeq 3.1d$, which corresponds to a slit thickness complying with the formation of three layers of complete spheres, but not thick enough to form spherical caps. Hence, we have an upper layer of tangent spheres with some eggplant defects. The interesting feature of this system is that within the planes the domains adopt an 2-D HEX packing, but when analyzing the 3-D packing, one observes that is not 3-D HEX, but closer to a (111) plane of face-centered cubic phase (FCC), since the first and the third layer are not superposed in the xy-plane. The

DOI: 10.1021/acs.macromol.5b02314
Macromolecules XXXX, XXX, XXX–XXX

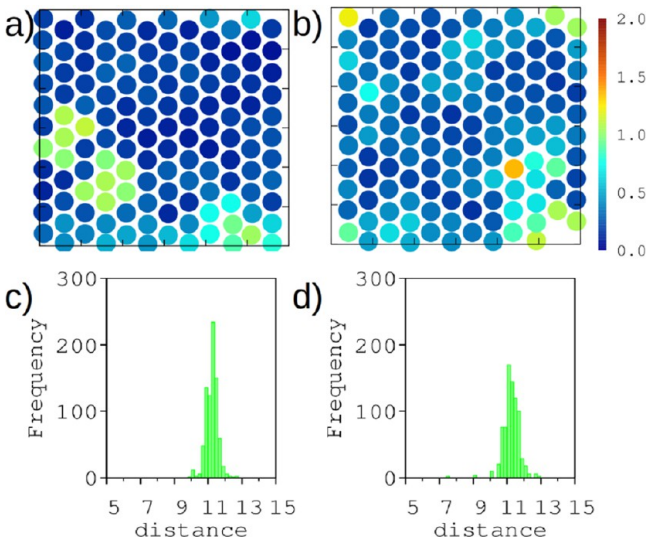

Figure 15. CDS simulations of sphere-forming BCP confined by solid surfaces. Bottom surface chemically activated with stripes attractive to A block and B block alternately and top surface neutral. Box size $L_x = L_y = 120$, $L_z = 24$ and stripes with a spacing of $L_S = 10$. Ratio of the Euclidean distance to HEX symmetry and distance to BCC symmetry (d_{HEX}/d_{BCC}): (a) lower layer; (b) upper layer. Histogram of the distances of each sphere with its six next-nearest neighbors: (d) lower layer; (e) upper layer.

packing density of both 3-D structures is, however, the same. Thus, the reason for the existence of this new structure could be that the equilibrium for such thickness is degenerated with two possible structures of maximum packing, namely, 3-D HEX and (111) FCC.

We have also analyzed systems of $L_z = 54 \simeq 4.9d$ and $56 \simeq 5.1d$ with the band periodicity $L_S = 10 \simeq L_0$, capable of allocating five layers of complete spheres, tangent to the upper wall or with spherical caps in it, respectively. The 3-D HEX order is maintained in the $L_z = 56$, with a plane separation approximately $\delta = 9.3$. As before, the system with tangent spheres, $L_z = 54$, produces (111) planes of a face-centered body, with $\delta \simeq 9.8$, and many eggplant defects at the upper layer. However, for $L_S = 12$ we obtain disordered systems for $n \geq 4$ layers of complete spheres, even with the appropriate L_z as given in eq 25, from both quenching and annealing routes.

4. CONCLUSIONS

In this article we have shown that the CDS is a powerful tool to predict the self-assembly of block copolymers into complex structures. Simulations of sphere-forming BCP on patterned surfaces confined in a slit have been compared with experimental data from Park et al.,[10] and an almost quantitative agreement is obtained. The comparison is done in terms of only one single characteristic length, namely, d, which is known to be physically proportional to a power of the size of the BCP $d \sim N^{2/3}$, in the strong segregation limit. The size of the domains of a given block seems to play a secondary role, provided that the domain geometry keeps being spherical.

Because of this inner simplicity of the problem, the structures that can be formed are rather limited by the bulk BCP equilibrium configuration and the hexagonal packing produced by the presence of a hard wall. The main result of this article lies in the fact that by tuning the band spacing of the chemically patterned surfaces together with the slit thicknesses, one of these two arrangements can be selected and produce long-range order structures, at least of the order of the size of the simulated systems. Along with the minimal distance between domains d, the system is sensitive to the band periodicity if the aim is at promoting a particular 3-D structure. In this way, if the band periodicity is approximately $L_0 = d\sqrt{3}/2$, the first layer of complete spheres (bottom up) is naturally hexagonal. It is additionally required, however, that the slit thickness is appropriate for a 3-D hexagonal cell to develop without conflict with upper surface constraint, as described in eq 24. On the contrary, if the band periodicity is approximately $2d/\sqrt{3}$ and the slit thickness is approximately given by eq 25, the system naturally develops a BCO structure already from the first layer. The latter result is a pure prediction of the CDS since no experiments have been done under these conditions yet, to the best of our knowledge. This fact is significantly different from what occurs in the presence of a nonpatterned lower surface, where the confining effect of the hard wall imposes a preference for a hexagonal structure.

We have also analyzed frustrated situations to explore the possibility of existence of exotic structures generated by the constraints, for the same physical system. On one hand, we have encountered hexagonally packed ordered systems with spheres tangent to the upper wall, formed on surface patterns with band periodicity $L_S = L_0$, by tuning the slit thickness to approximately that of eq 26. This type of situation has been also observed in the experiments. For this type of frustration, the layer separation $\delta > d\sqrt{2/3}$ as it would correspond to the perfect 3-D HEX. This effect can be caused by the presence of eggplant defects, which are deformed domains cut by the upper wall, to favor the conformation of the BCP chains near the wall, pulling the whole system up. On the other hand, we also have studied systems whose thickness is in between the values given by eqs 24 and 26, both with $n = 2$ layers of complete spheres. We have analyzed only the case $L_S = L_0$. We have observed that the first and second layers have a clear structure of a (110) plane of a BCC instead of an expected HEX, probably due to a subtle effect of the bands on the possible displacements of the spheres under changing external conditions, which deserves further investigation. This case shows a distance between the layers slightly compressed $\delta < d\sqrt{2/3}$, which can be attributed to the presence of incomplete spheres, cut by the wall between its pole and equator, that push the whole system down. Hence, the fine-tuning of the slit thickness is also of crucial importance to obtain the desired ordered 3-D structures.

The analysis carried out in this article suggests that the use of chemical masks on surfaces, together with the control of the thickness can be a useful tool to create the desired structure from the self-assembly of BCP. We believe that this is a step forward toward the applications of this systems in well-controlled fabrication of nanoscopic devices.

■ ASSOCIATED CONTENT

Supporting Information

The Supporting Information is available free of charge on the ACS Publications website at DOI: 10.1021/acs.macromol.5b02314.

Qualitative analysis of the system and Euclidean distance between structures (ZIP)

DOI: 10.1021/acs.macromol.5b02314
Macromolecules XXXX, XXX, XXX−XXX

AUTHOR INFORMATION

Corresponding Authors

*E-mail: josep.bonet@urv.cat (J.B.A.).
*E-mail: mpinna@lincoln.ac.uk (M.P.).

Notes

The authors declare no competing financial interest.

ACKNOWLEDGMENTS

M.S. thanks the Spanish Ministrerio of Educación, Cultura y Deporte (Grant AP2010-2150). Moreover, M.S. thanks A.Z. and M.P. for the hospitality during her stay at the Computational Physics group, which includes the access to the CDS code and resources during part of the research stay, as well as the scientific assistance of the members of the group, where this research was initiated. M.S. and J.B.A. are grateful for that.

REFERENCES

(1) Fasolka, M. J.; Mayes, A. M. *Annu. Rev. Mater. Res.* **2001**, *31*, 323.
(2) Hamley, I. W. *Nanotechnology* **2003**, *14*, R39−R54.
(3) Park, C.; Yoon, J.; Thomas, E. L. *Polymer* **2003**, *44*, 6725.
(4) Muller, M.; Sun, D. *Phys. Rev. Lett.* **2013**, *111*, 267801.
(5) Park, M.; Harrison, C.; Chaikin, P. M.; Register, R. A.; Adamson, D. *Science* **1997**, *276*, 1401.
(6) Thurn-Albrecht, T.; Schotter, J.; Kastle, G.; Emley, N.; Stubauchui, T.; Krusin-Elbaum, L.; Black, C.; Tuominen, M.; Russell, T. *Science* **2000**, *290*, 2126.
(7) Segalman, R. A. *Mater. Sci. Eng., R* **2005**, *48*, 191.
(8) Hamley, I. W. *Prog. Polym. Sci.* **2009**, *34*, 1161−1210.
(9) Kim, J. K.; Yang, S. Y.; Lee, Y.; Kim, Y. *Prog. Polym. Sci.* **2010**, *35*, 1325−1349.
(10) Park, S.-M.; Craig, G. S. W.; La, Y.-H.; Nealey, P. F. *Macromolecules* **2008**, *41*, 9124−9129.
(11) Bates, F. S.; Fredrickson, G. H. *Annu. Rev. Phys. Chem.* **1990**, *41*, 525.
(12) Matsen, M. W.; Bates, F. S. *Macromolecules* **1996**, *29*, 1091−1098.
(13) Hamley, I. W. *The Physics of Block Copolymers*; Oxford University Press: Oxford, 1998.
(14) Fredrickson, G. H. *Macromolecules* **1987**, *20*, 2535−2542.
(15) Wang, Q. In *Nanostructured Soft Matter: Experiment, Theory, Simulation, and Perspectives*; Zvelindovsky, A. V., Ed.; Springer: Dordrecht, 2007; pp 495−528.
(16) Shi, A.-C.; Li, B. In *Polymer Science: A Comprehensive Reference*; Matyjaszewski, K., Muller, M., Eds.; Elsevier: Amsterdam, 2012; pp 71−81.
(17) Shin, K.; Xiang, H.; Moon, S. I.; Kim, T.; McCarthy, T. J.; Russell, T. P. *Science* **2004**, *306*, 76.
(18) Wu, Y.; Chen, G.; Katsov, K.; Sides, S. W.; Wang, J.; Tang, J.; Fredrickson, G. H.; Moskovits, M.; Stucky, G. D. *Nat. Mater.* **2004**, *3*, 816.
(19) Dobriyal, P.; Xiang, H.; Kazuyuki, M.; Chen, J.-T.; Jinnai, H.; Russell, T. P. *Macromolecules* **2009**, *42*, 9082−9088.
(20) Wang, Y.; Qin, Y.; Berger, A.; Yau, E.; He, C.; Zhang, L.; Gosele, U.; Knez, M.; Steinhart, M. *Adv. Mater.* **2009**, *21*, 2763−2766.
(21) Arsenault, A. C.; Rider, D. A.; Tetreault, N.; Chen, J. I.-L.; Coombs, N.; Ozin, G. A.; Manners, I. *J. Am. Chem. Soc.* **2005**, *127*, 9954−9955.
(22) Kellogg, G. J.; Walton, D. G.; Mayes, A. M.; Lambooy, P.; Russell, T. P.; Gallagher, P. D.; Satija, S. K. *Phys. Rev. Lett.* **1996**, *76*, 2503.
(23) Koneripalli, N.; Levicky, R.; Bates, F. S.; Ankner, J.; Kaiser, H.; Satija, S. K. *Langmuir* **1996**, *12*, 6681−6690.
(24) Huang, E.; Russell, T. P.; Harrison, C.; Chaikin, P. M.; Register, R. A.; Hawker, C. J.; Mays, J. *Macromolecules* **1998**, *31*, 7641.
(25) Knoll, A.; Horvat, A.; Lyakhova, K. S.; Krausch, G.; Sevink, G. J. A.; Zvelindovsky, A. V.; Magerle, R. *Phys. Rev. Lett.* **2002**, *89*, 035501.
(26) Yokoyama, H.; Mates, T. E.; Kramer, E. J. *Macromolecules* **2000**, *33*, 1888−1898.
(27) Segalman, R. A.; Hexemer, A.; Kramer, E. J. *Phys. Rev. Lett.* **2003**, *91*, 196101.
(28) Angelescu, D. E.; Harrison, C. K.; Trawick, M. L.; Register, R. A.; Chaikin, P. M. *Phys. Rev. Lett.* **2005**, *95*, 025702.
(29) Kramer, E. J. *Nature* **2005**, *437*, 824−825.
(30) Li, W.; Muller, M. *Annu. Rev. Chem. Biomol. Eng.* **2015**, *111*, 267801.
(31) Kim, H.-C.; Hinsberg, W. D. *J. Vac. Sci. Technol., A* **2008**, *26*, 1369−1382.
(32) Rockford, L.; Liu, Y.; Mansky, P.; Russell, T. P.; Yoon, M.; Mochrie, S. *Phys. Rev. Lett.* **1999**, *82*, 2602.
(33) Yang, X. M.; Peters, R. D.; Nealey, P. F.; Solak, H. H.; Cerrina, F. *Macromolecules* **2000**, *33*, 9575−9582.
(34) Kim, S. O.; Solak, H. H.; Stoykovich, M. P.; Ferrier, N. J.; Pablo, J. J.; Nealey, P. F. *Nature* **2003**, *424*, 411.
(35) Edwards, E. W.; Muller, M.; Stoykovich, M. P.; Solak, H. H.; de Pablo, J. J.; Nealey, P. F. *Macromolecules* **2007**, *40*, 90−96.
(36) Kim, H.; Daniels, E. S.; Li, S.; Mokkapati, V. K.; Kardos, K. *J. Polym. Sci., Part A: Polym. Chem.* **2007**, *45*, 1038−1054.
(37) Ruiz, R.; Kang, H.; Detcheverry, F. A.; Dobisz, E.; Kercher, D. S.; Albrecht, T. R.; de Pablo, J. J.; Nealey, P. F. *Science* **2008**, *321*, 936.
(38) Tada, Y.; Akasaka, S.; Yoshida, H.; Hasegawa, H.; Dobisz, E.; Kercher, D.; Takenaka, M. *Macromolecules* **2008**, *41*, 9267−9276.
(39) Ji, S.; Nagpal, U.; Liao, W.; Liu, C.-C.; de Pablo, J. J.; Nealey, P. F. *Adv. Mater.* **2011**, *23*, 3692−3697.
(40) Park, S.-M.; Craig, G. S. W.; La, Y.-H.; Solak, H. H.; Nealey, P. F. *Macromolecules* **2007**, *40*, 5084.
(41) Segalman, R.; Yokoyama, H.; Kramer, E. J. *Adv. Mater.* **2001**, *13*, 1152−1155.
(42) Chuang, V. P.; Cheng, J. Y.; Savas, T. A.; Ross, C. A. *Nano Lett.* **2006**, *6*, 2332−2337.
(43) Bita, I.; Yang, J. K. W.; Jung, Y. S.; Ross, C. A.; Thomas, E. L.; Berggren, K. K. *Science* **2008**, *321*, 939.
(44) Xiao, S.; Yang, X.; Park, S.; Weller, D.; Russell, T. P. *Adv. Mater.* **2009**, *21*, 2516−2519.
(45) Stein, G. E.; Kramer, E. J.; Li, X.; Wang, J. *Macromolecules* **2007**, *40*, 2453−2460.
(46) Wu, M. W.; Register, R. A.; Chaikin, P. M. *Phys. Rev. E* **2006**, *74*, 040801(R).
(47) Xu, J.; Park, S.; Wang, S.; Russell, T. P.; Ocko, B. M.; Checco, A. *Adv. Mater.* **2010**, *22*, 2268.
(48) Ye, X.; Edwards, B. J.; Khomami, B. *Macromol. Rapid Commun.* **2012**, *33*, 392−395.
(49) Ramírez-Hernández, A.; Liu, G.; Nealey, P. F.; de Pablo, J. J. *Macromolecules* **2012**, *45*, 2588−2596.
(50) Liu, G.; Detcheverry, F.; Ramírez-Hernández, A.; Yoshida, H.; Tada, Y.; de Pablo, J. J.; Nealey, P. F. *Macromolecules* **2012**, *45*, 3986−3992.
(51) Chen, P.; Liang, H.; Xia, R.; Qian, J.; Feng, X. *Macromolecules* **2013**, *46*, 922−926.
(52) Liu, C.-C.; Ramírez-Hernández, A.; Han, E.; Craig, G. S. W.; Tada, Y.; Yoshida, H.; Kang, H.; Ji, S.; Gopalan, P.; de Pablo, J. J.; Nealey, P. F. *Macromolecules* **2013**, *46*, 1415−1424.
(53) Matsen, M. W. *J. Chem. Phys.* **1997**, *106*, 7781.
(54) Drolet, F.; Fredrickson, G. H. *Phys. Rev. Lett.* **1999**, *83*, 4317−4320.
(55) Bosse, A. W.; Garcia-Cervera, C. J.; Fredrickson, G. H. *Macromolecules* **2007**, *40*, 9570.
(56) Hur, S. M.; Garcia-Cervera, C. J.; Kramer, E. J.; Fredrickson, G. H. *Macromolecules* **2009**, *42*, 5861.
(57) Trombly, D. M.; Pryamitsyn, V.; Ganesan, V. *J. Chem. Phys.* **2011**, *134*, 154903.
(58) Petera, D.; Muthukumar, M. *J. Chem. Phys.* **1998**, *109*, 5101−5107.
(59) Yang, G.; Tang, P.; Yang, Y.; Cabral, J. T. *J. Phys. Chem. B* **2009**, *113*, 14052−14061.

DOI: 10.1021/acs.macromol.5b02314
Macromolecules XXXX, XXX, XXX−XXX

(60) Ye, X.; Edwards, B. J.; Khomami, B. *Macromolecules* **2010**, *43*, 9594−9597.
(61) Kriksin, Y. A.; Neratova, I. V.; Khalatur, P. G.; Khokhlov, A. R. *Chem. Phys. Lett.* **2010**, *492*, 103−108.
(62) Wang, Q.; Nath, S. K.; Graham, M. D.; Nealey, P.; de Pablo, J. J. *J. Chem. Phys.* **2003**, *118*, 11278.
(63) Wang, Q.; Nealey, P. F.; de Pablo, J. J. *Macromolecules* **2003**, *36*, 1731−1740.
(64) Detcheverry, F. A.; Pike, D. Q.; Nagpal, U.; Nealey, P. E.; de Pablo, J. J. *Phys. Rev. Lett.* **2009**, *102*, 197801.
(65) Nagpal, U.; Muller, M.; Nealey, P. F.; de Pablo, J. J. *ACS Macro Lett.* **2012**, *1*, 418.
(66) Ohta, T.; Kawasaki, K. *Macromolecules* **1986**, *19*, 2621.
(67) Oono, Y.; Puri, S. *Phys. Rev. Lett.* **1987**, *58*, 836.
(68) Hamley, I. W. *Macromol. Theory Simul.* **2000**, *9*, 363.
(69) Pinna, M.; Zvelindovsky, A. V. *Eur. Phys. J. B* **2012**, *85*, 210.
(70) Chakrabarti, A.; Chen, H. *J. Polym. Sci., Part B: Polym. Phys.* **1998**, *36*, 3127.
(71) Chen, L. Q.; Shen, J. *Comput. Phys. Commun.* **1998**, *108*, 147.
(72) Feng, J.; Liu, H.; Hu, Y. *Macromol. Theory Simul.* **2002**, *11*, 549.
(73) Feng, J.; Liu, H.; Hu, Y. *Macromol. Theory Simul.* **2002**, *11*, 556.
(74) Li, W.; Qiu, F.; Yang, Y.; Shi, A.-C. *Macromolecules* **2010**, *43*, 1644.
(75) Li, W.; Xie, N.; Qiu, F.; Yang, Y.; Shi, A.-C. *J. Chem. Phys.* **2011**, *134*, 144901.
(76) Ohta, T.; Enomoto, Y.; Harden, J. L.; Doi, M. *Macromolecules* **1993**, *26*, 4928.
(77) de Groot, S. R.; Mazur, P. *Phys. Rev.* **1954**, *94*, 218−224.
(78) Fredrickson, G. H.; Helfand, E. *J. Chem. Phys.* **1987**, *87*, 697−705.
(79) Qi, S.; Wang, Z.-G. *Phys. Rev. E: Stat. Phys., Plasmas, Fluids, Relat. Interdiscip. Top.* **1997**, *55*, 1682.
(80) Zvelindovsky, A. V.; Zatovsky, A. V. *Il Nuovo Cimento D* **1997**, *19*, 725−745.
(81) van Vlimmeren, B. A. C.; Maurits, N. M.; Zvelindovsky, A. V.; Sevink, G. J. A.; Fraaije, J. G. E. M. *Macromolecules* **1999**, *32*, 646−656.
(82) Knoll, A.; Lyakhova, K. S.; Horvat, A.; Krausch, G.; Sevink, G. J. A.; Zvelindovsky, A. V.; Magerle, R. *Nat. Mater.* **2004**, *3*, 886−890.
(83) Horvat, A.; Sevink, G. J. A.; Zvelindovsky, A. V.; Krekhov, A.; Tsarkova, L. *ACS Nano* **2008**, *2*, 1143−1152.
(84) Bahiana, M.; Oono, Y. *Phys. Rev. A: At., Mol., Opt. Phys.* **1990**, *41*, 6763.
(85) Leibler, L. *Macromolecules* **1980**, *13*, 1602.
(86) Ren, S. R.; Hamley, I. W. *Macromolecules* **2001**, *34*, 116.
(87) Marko, J. F. *Phys. Rev. E: Stat. Phys., Plasmas, Fluids, Relat. Interdiscip. Top.* **1993**, *48*, 2861.
(88) Feng, J.; Ruckenstein, E. *J. Chem. Phys.* **2004**, *121*, 1609.
(89) Ren, S. R.; Hamley, I. W.; Sevink, G. J. A.; Zvelindovsky, A. V.; Fraaije, J. G. E. M. *Macromol. Theory Simul.* **2002**, *11*, 123.
(90) Shinozaki, A.; Oono, Y. *Phys. Rev. E: Stat. Phys., Plasmas, Fluids, Relat. Interdiscip. Top.* **1993**, *48*, 2622.
(91) Ren, S. R.; Hamley, I. W.; Teixeira, P. I. C.; Olmsted, P. D. *Phys. Rev. E: Stat. Phys., Plasmas, Fluids, Relat. Interdiscip. Top.* **2001**, *63*, 041503.
(92) Pinna, M.; Zvelindovsky, A. V.; Todd, S.; Goldbeck-Wood, G. *J. Chem. Phys.* **2006**, *125*, 154905.
(93) Pinna, M.; Zvelindovsky, A. V.; Guo, X.; Stokes, C. L. *Soft Matter* **2011**, *7*, 6991.
(94) Vega, D. A.; Harrison, C. K.; Angelescu, D. E.; Trawick, M. L.; Huse, D. A.; Chaikin, P. M.; Register, R. A. *Phys. Rev. E* **2005**, *71*, 061803.
(95) Komura, S.; Fukuda, J.-I.; Paquette, G. C. *Phys. Rev. E: Stat. Phys., Plasmas, Fluids, Relat. Interdiscip. Top.* **1996**, *53*, R5588.
(96) Brazovskii, S. A. *Sov. Phys. JETP* **1975**, *41*, 85.
(97) Stein, G. E.; Cochran, E. W.; Katsov, K.; Fredrickson, G. H.; Kramer, E. J.; Li, X.; Wang, J. *Phys. Rev. Lett.* **2007**, *98*, 158302.

DOI: 10.1021/acs.macromol.5b02314
Macromolecules XXXX, XXX, XXX−XXX